20-Dimensional surrogate-assisted Bayesian optimization of laser-driven proton beams

Elias Catrix*,[1] Sylvain Fourmaux,[1] Simon Vallières,[1] François Bianchi,[1] François Fillion-Gourdeau,[2,1] Joël Maltais,[1] Steve MacLean,[2,1] and Patrizio Antici*[1]

[1)] *Institut national de la recherche scientifique, 1650 blvd. Lionel-Boulet, Varennes, Quebec J3X 1P7, Canada*

[2)] *Infinite Potential Laboratories, Waterloo, N2L 0A9 Ontario, Canada*

(*Electronic mail: elias.catrix@inrs.ca, patrizio.antici@inrs.ca)

(Dated: 23 May 2025)

Laser-driven proton acceleration, as obtained by the interaction of a high-intensity laser with matter, is a promising technique for generating high-quality proton beams. One of the main challenges is increasing the maximum proton energy. Here, we demonstrate a 70% increase in the maximum energy of laser-driven protons by optimizing the wavefront of the intense laser using Machine Learning: This was accomplished through adaptive control of a deformable mirror (DM) using a multi-step Random Forest surrogate-assisted Bayesian optimization approach. Starting from zeroed DM actuator voltages, our method identified an optimal configuration using 20 out of 48 actuators, requiring fewer than 150 experimental data samples. Our method surpassed conventional wavefront correction by 24%, which typically minimizes aberrations to converge toward a flat wavefront by leveraging real-time feedback from a wavefront sensor. This data-driven method integrating advanced wavefront control challenges the preference for correcting aberrations to achieve a flatter wavefront in laser-driven ion acceleration. We also propose a strategy for optimizing short focal length ion accelerators at facilities where measuring the wavefront at nominal full laser power is not implemented.

Laser-driven proton acceleration is a promising technique for generating high-energy proton beams with applications in medicine[1–3], material science[4,5], cultural heritage[6–9], fusion[10–12] and high-energy physics[13–17]. Among laser-driven ion acceleration techniques, Target Normal Sheath Acceleration (TNSA) permits the production of ultra-short proton bursts with high peak energies[18]. However, stable and repeatable high-brightness beams remain challenging to achieve due to an unstable laser-plasma interaction that impacts particle numbers, energies, and the divergence profile. Precise laser parameter control is essential to optimize these complex interactions.

Machine Learning (ML) has recently gained interest as a data-driven approach for exploring complex parameter spaces in experimental physics[19–21]. By efficiently guiding the search for optimal conditions, it offers a promising avenue for improving laser-based particle acceleration. This approach leverages real-time diagnostics and predictive modeling to refine experimental parameters with minimal iterations. Recent work underscores the expanding use of ML in laser–plasma optimization, from surrogate modeling for phase-stable acceleration[22] to synthetic diagnostics predicting proton spectra via deep learning[23].

Bayesian optimization (BO)[24–27] has proven effective for optimizing computationally or experimentally intensive, noisy, black-box objective functions in low-dimensional parameter spaces (typically ≤ 20)[28]. BO builds a probabilistic model, usually a Gaussian Process (GP), of the objective function — here the maximum proton energy — allowing efficient sampling of points. This probabilistic BO technique has been used to maximize the pulse energy at the LCLS x-ray free-electron laser facility[29] and improve the electron beam quality in laser wakefield electron acceleration[30–33]. However, its application for laser-driven proton acceleration remains relatively underexplored[34], largely due to the limited repetition rates[35–40] of ion beamlines and the noisy data resulting from non-linear laser-plasma interactions[41,42].

The laser spot size and shape are crucial for efficient laser-driven ion acceleration and depend on the wavefront profile. Conventional wavefront correction methods, guided by wavefront sensors, can improve beam quality[43–45], often optimizing towards Gaussian profiles and flat wavefronts. However, several groups have demonstrated superior performances using non-Gaussian beams[46–48], hence these wavefront correction methods face challenges in navigating the complex parameter space of ion acceleration as they don't directly optimize the final ion beam parameters, like the maximum energy.

In this work, we introduce a data-driven approach that combines advanced wavefront control with a multi-step Bayesian optimization process (MSBO) to enhance the maximum kinetic energy of laser-driven proton beams in the TNSA regime. This framework leverages the control of deformable mirror (DM) actuators to systematically explore different wavefront configurations, challenging conventional assumptions about optimal laser beam profiles for TNSA. This technique is also practical for laser facilities lacking terawatt/petawatt attenuators, where direct laser spot visualization and wavefront measurement at full power are impractical.

Experiments were conducted on the laser-driven ion acceleration beamline at the Institut national de la recherche scientifique (INRS) in Varennes, Canada, using the ALLS 150 TW Ti:Sapphire laser[49]. This double chirped-pulsed amplified (CPA) system delivers 3.2 J on target with a pulse duration of $\tau_{\mathrm{FWHM}} = 22$ fs (Full-Width-Half-Maximum) and a central wavelength of $\lambda_0 = 800$ nm. The experimental setup, illustrated in Figure 1.A, employs an $f/3$ off-axis parabola (OAP) to focus the 95 mm diameter beam (measured at e^{-2}) down to a focal spot size of $w_{\mathrm{FWHM}} \sim 5\ \mu$m, achieving a peak intensity I_0 of approximately 1.3×10^{20} W/cm^2. Before laser pulse compression the beam underwent a cross-wave polarizer

(XPW) cleaning, ensuring an Amplified Spontaneous Emission (ASE) pre-pulse contrast of $< 10^{-10}$ at -100 ps relative to the main pulse and a steep power rise with a contrast of $< 10^{-6}$ at -3 ps. A piezoelectric bimorph DM with 48 actuators from *AKAOptics* (with a maximum voltage range [-200 V, +200V]), shown in Figure 1.B, allowing for precise wavefront shaping, and a *SID4* wavefront sensor (WFS) from *Phasics* provided real-time feedback to assess quantitatively the impact of DM actuator configurations on the laser beam wavefront. At the same time, a CCD camera was used for beam visualization at the focus position. This beam analysis is performed at the laser nominal energy of 3.2 J by attenuating the laser beam energy with wedges before the diagnostics.

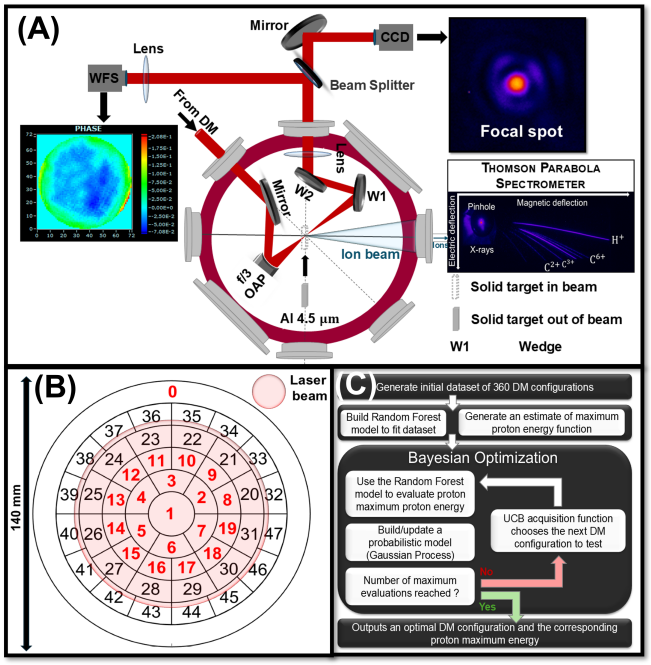

FIG. 1. (A) Sketch of the experimental setup including direct visualization of the laser focus and laser wavefront real-time diagnostics both measured at maximum laser energy (3.2 J). (B) Deformable mirror actuators' map. (C) Diagram of the MSBO approach used to optimize the proton maximum energy.

The experiment utilized p-polarized laser pulses incident at a 20° angle relative to the target normal on a 4.5-μm-thick aluminum foil to generate ion beams via the TNSA regime. The target, mounted on a multi-target holder accommodating up to 400 targets, was positioned at the laser focus, enabling systematic and efficient experimentation at a repetition rate of 0.625 Hz[40]. A Thomson parabola spectrometer coupled with a microchannel plate (MCP) detector was employed to measure the proton spectrum and record the maximum proton energy at every laser shot. This energy is defined as the proton energy located at the midpoint of the cutoff energy slope in the spectrum. The shot-to-shot variation of the maximum proton energy was typically around 5%, which is a crucial factor in this study, as the noise introduced by the optimization process is directly linked to the inherent stability of the TNSA mechanism. More information on the setup can be found in Catrix et al. and Vallières et al.[40,49].

To maximize the proton energies, we implemented a multi-step approach based on a Random Forest (RF) model[50] and BO (Figure 1.C). RF was selected for its ability to capture complex non-linear relationships and handle noisy, high-dimensional data. RF has proven highly effective in both accurate prediction and physical interpretability, making them valuable tools for disruption classification and hybrid physics machine learning models in plasma stability forecasting[51,52]. In this study, RF is used to approximate and predict the maximum proton energy as a function of input actuator voltages while BO is used to find the maximal energy.

First, a dataset of 360 DM actuator configurations was generated using Latin Hypercube Sampling[53,54] (LHS) by independently varying the voltages of actuators 0 to 19 within [-80 V, 80 V]. The remaining actuators were set to 0 V. LHS ensures diverse, well-distributed parameter coverage. The correlation matrix reveals a strong positive correlation (0.86) between actuator 0, which controls the laser pulse defocus, and the maximum proton energy, indicating its primary influence. Most actuators exhibit weaker correlations suggesting lower impact than electrode 0, with an average correlation of (0.08). Moreover, the correlation matrix indicates weak inter-actuator correlations ($< |0.1|$), showing that most actuators function independently with minimal mutual influence.

In the second step, an RF model is trained on the initial dataset to estimate the relationship between 20 DM actuators and the maximum proton energy. Using 300 decision trees, predictions are made with robustness and noise reduction. In the algorithm, the trees grow until the leaves are pure. A pure leaf, in this context, means that a set of actuator voltages results in the same proton energy output.

In the third step, BO was performed using Python's *gpminimize* function from *scikit-optimize* package[55], with the trained RF model as the objective function. This GP-based method iteratively refined predictions by balancing exploration (sampling uncertain regions) and exploitation (focusing on promising configurations). The Upper Confidence Bound (UCB) acquisition function helped to efficiently navigate the high-dimensional, noisy search space, prioritizing high-energy or uncertain configurations.

In the final step, BO located an optimized DM configuration and its corresponding maximum proton energy was predicted by the RF model. The optimized DM configuration was then tested experimentally to assess the efficiency of our method. BO has the main advantage of minimizing resource-intensive experiments while systematically identifying optimal actuator settings, demonstrating BO's effectiveness. Indeed, by optimizing directly within real experimental conditions, BO can adapt to shifts, such as TNSA target misalignments, ensuring maximized proton energy without relying on indirect wavefront measurements.

Optimal values of a trained RF model can be found using random search, grid search, or optimization algorithms. BO was chosen for its efficiency in complex, high-dimensional spaces, guiding the search toward promising regions for maximizing proton energy. This iterative approach significantly reduces evaluations needed to converge to an optimal solution

compared to an exhaustive random or grid search.

In low-repetition-rate experimental contexts, where each laser shot is time-consuming and resource-intensive, reducing the number of experimental evaluations is essential. BO offers an effective framework for this, even when paired with fast-to-evaluate surrogate models like RF. By using a trained Random Forest model, BO can efficiently explore the search space without needing real experiments at each step, saving significant time and cost. The RF model handles noisy experimental data well and enables rapid evaluations, supporting robust offline optimization that smooths out noise and can ignore failed shots. It also reduces the risks of damaging configurations during live runs — like extreme voltages that could damage optics — by decoupling optimization from the experiment. This not only accelerates the search for optimal configurations but also facilitates safer and more flexible implementation. Our approach is well-aligned with established methods in the literature, such as Sequential Model-Based Algorithm Configuration[56] and Efficient Global Optimization[24], which demonstrate the power of surrogate-assisted optimization in high-dimensional, costly-to-evaluate settings.

A comparison of experimental proton spectra for three actuator configurations is shown in Figure 2.A. The maximum proton energy increased by ∼70%, reaching $E_{\mathrm{pmax}} = (6.64 \pm 0.30)$ MeV with the MSBO-determined optimal DM configuration. This represents a significant improvement over the zeroed DM configuration, which yielded $E_{\mathrm{pmax}} = (3.85 \pm 0.14)$ MeV. MSBO also outperforms conventional wavefront correction methods, which optimizes the laser beam towards a flat wavefront, by ∼24% ($E_{\mathrm{pmax}} = (5.37 \pm 0.24)$ MeV), demonstrating the superior performance of the MSBO-optimized configuration. Unlike MSBO, traditional wavefront correction lacks proton beam feedback when relying solely on the *SID4* WFS.

The results reveal that the highest maximum proton energy consistently corresponds to a deformed wavefront, as shown in Figure 2. B-D, which present beam profiles without corrections, with WFS-based optimization, and with MSBO, respectively. Notably, maximum proton energy is achieved without maximizing laser intensity on the target. Figure 2.E highlights focal spot differences under identical conditions (same camera settings and gain). These findings suggest that BO optimizes proton acceleration by shaping the wavefront for a more favorable laser-plasma interaction, even with lower peak intensity and broader width than WFS-based optimization. While the Fuchs et al.[57] model predicts a lower hot electron temperature for the MSBO configuration due to a lower peak intensity, our data show that MSBO generates hotter electrons and higher cutoff energy, underscoring the model's limits at ultrahigh intensities and short pulse durations where multidimensional and time-dependent effects matter.

To evaluate the efficiency and reliability of the optimization process, we conducted 89 consecutive optimization trials, each one using a different RF predictive model trained on a randomly selected and size-increased subset of 2 to 358 laser shots from the initial dataset (2, 6, 10, 14 ... up to 358). Each optimization trial was repeated 10 times for statistical robustness, tracking the global maximum predicted by

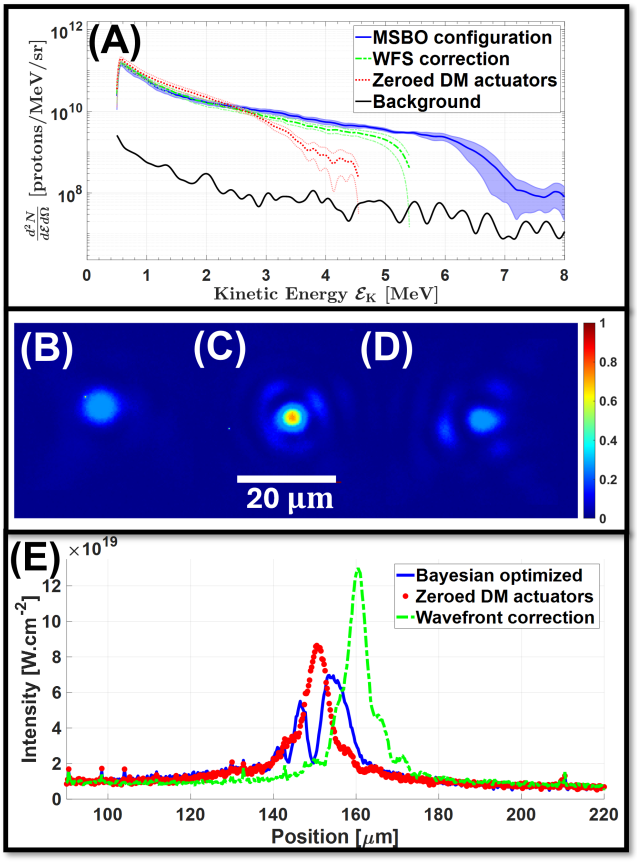

FIG. 2. (A) Average proton spectra over 10 shots under different optimization conditions; The window has been cut to 8 MeV for visualization purposes but we can measure proton energies currently up to 12 MeV[49]; Error bars are calculated using the standard deviation over 10 laser shots. Focal spots with (B) no wavefront correction, (C) optimized towards a flat wavefront using a WFS, and (D) optimized with MSBO. (E) Comparison of focal spot transverse (horizontal) profiles for 3 wavefront optimization strategies. The intensity is plotted as a function of position for three different cases: MSBO (solid blue), no correction (dotted red), and WFS correction (dashed green).

the GP model at each iteration. All runs started with DM actuator voltages set to 0 V. Figure 3.A shows the mean (blue curve) and standard deviation (shaded sky blue curve) of the predicted optima across ten runs, illustrating the evolution of E_{pmax} as a function of the number of laser shots. Initially, E_{pmax} is ∼3 MeV for ∼5 shots, rising sharply to ∼90% of its final value within 30 shots and reaching 6 MeV around 50 shots. The growth then slows down, stabilizing around 6.2 MeV after about 100 shots, with minor fluctuations up to 358 shots. This suggests that 100-150 shots suffice to determine an optimal DM configuration and reliably estimate $E_{\mathrm{pmax}} = (6.44 \pm 0.33)$ MeV, closely matching the experimental value ($E_{\mathrm{pmax}} = (6.64 \pm 0.30)$ MeV). The shaded region represents uncertainty, which is initially higher due to limited data but which is narrowing as more shots improve the model confidence. This analysis highlights the trade-off between data acquisition and predictive accuracy, crucial for op-

timizing experiments. The entire process, including dataset collection, parameter setting, and computation (5 minutes), took ∼1 hour. In comparison, manual and wavefront correction methods require at least a similar timeframe but yield suboptimal results. Optimizing only actuator 0, which correlates most with E_{pmax}, resulted in $E_{\mathrm{pmax}} = (5.25 \pm 0.22)$ MeV, demonstrating the advantage of high-dimensional wavefront control in laser-plasma acceleration.

In Figure 3.B, we represent the evolution of the Root Mean Square Error (RMSE) of RF predictive models as a function of the number of laser shots used to train and test the model. The RMSE is a commonly used metric in ML indicating the model's predictive performance. It is defined as:

$$\mathrm{RMSE} = \sqrt{\frac{1}{n}\sum_{i=1}^{n}(y_i - \hat{y}_i)^2}, \tag{1}$$

where n is the number of laser shots, y_i are the actual (experimentally measured) maximum proton energy values, and $\hat{y}_i$ are the predicted maximum proton energy values.

Here, RMSE is computed on experimental test datasets (15% of the initial data) to evaluate model error and optimization convergence. Initially high (∼1.3 MeV for <10 shots) with large fluctuations due to limited training data, RMSE decreases rapidly, falling below 0.5 MeV around 50 shots. Beyond ∼100 shots, it stabilizes at 0.25 to 0.35 MeV, with minor fluctuations up to 358 shots, indicating that additional data beyond this threshold yield minimal accuracy gains. The residual noise (∼ ±0.3 MeV) at higher shot numbers likely stems from inherent experimental measurement noise, in particular shot-to-shot fluctuations[40].

For MSBO to be effective, source stability is crucial, as experimental noise inherently limits prediction accuracy. Indeed, the experimental standard deviation, the standard deviation of the predicted maximum energy, and the RMSE of the RF model, are all of the same order (∼5%), indicating that the model's predictive accuracy is well-aligned with the shot-to-shot fluctuations.

In our case, each target-holder allows for approximately 400 shots before target-holder replacement, with the optimization process requiring ∼150 shots, leaving 250 for further studies. Even with only 50–100 shots, MSBO maintains good performance while preserving more shots for additional studies. Testing the MSBO-determined DM configuration on a new target-holder resulted in a lower maximum proton energy ($E_{\mathrm{pmax}} = (5.82 \pm 0.38)$ MeV), a 13% reduction, with minimal misalignment effects. This decline is likely due to target surface quality, alignment variations, or long-term laser energy drift, which can reach ∼10% if unadjusted during an experiment.

The superior performance of non-flat wavefronts optimized via DM configurations over traditional flat profiles in laser-driven ion acceleration suggests that unconventional beam profiles could unlock new operational regimes in laser-plasma interactions. This matches with prior findings where ion acceleration optimization was achieved through advanced control techniques without maximizing on-target laser intensity[34]. Beyond peak intensity, factors such as:

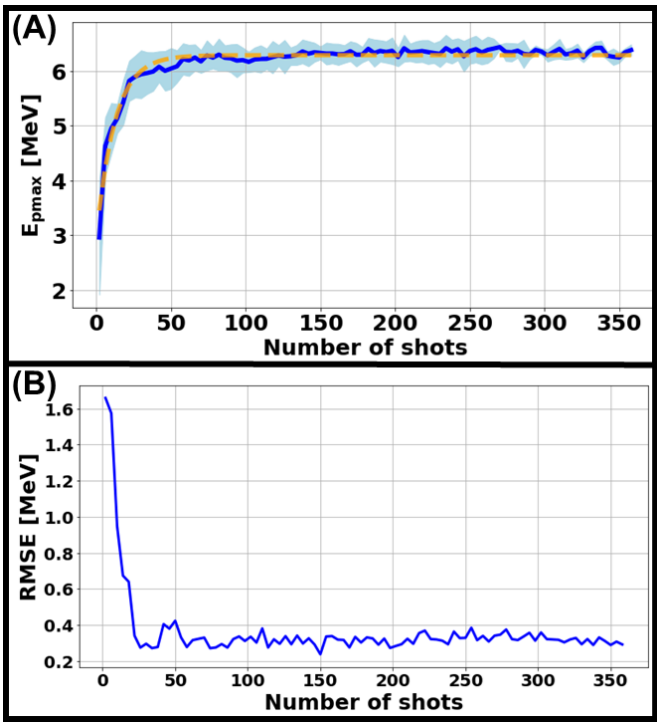

FIG. 3. (A) Average convergence plot for maximum estimated proton energy selecting successively and randomly 1 to 360 data samples to build the predictive model, over 10 runs of MSBO. (B) Evolution of the Root Mean Square Error (RMSE) of the predictive model as a function of shots used to train and test the model.

wavefront shaping parameter tuning, and spatiotemporal profiles; play a crucial role in enhancing acceleration. Recent studies favor novel laser modes, such as Laguerre–Gaussian (LG) beams[46,47], which enhance proton acceleration by reducing divergence and improving energy deposition. Camilla Willim et al.[48] investigate the use of high-intensity twisted laser beams — specifically, LG modes carrying orbital angular momentum — to produce collimated proton bunches with energies up to 40 MeV and a divergence approximately 6.5 times smaller than those driven by conventional Gaussian laser beams of the same energy. In fact, LG beams enhance hot electron production, leading to higher proton energies, likely due to a structured intensity distribution improving energy coupling into plasma electrons. This structured intensity profile, similar to ours, may reduce hot electron divergence, keeping more electrons near the propagation axis and ensuring a uniform sheath field for efficient proton acceleration. The fundamental Gaussian mode contributes ∼28.6% of the MSBO beam energy, with ∼91% in azimuthally symmetric modes, indicating preserved cylindrical symmetry despite deviations from a pure Gaussian.

Our findings demonstrate how non-Gaussian laser modes improve energy coupling to plasma, enhancing ion beam characteristics. Understanding the specific focal spot shape emerging from this optimization would require costly 2D–3D simulations to investigate its influence on energy transfer and plasma dynamics in the TNSA process. While such studies

could provide deeper insights, this paper primarily demonstrates MSBO's effectiveness in tuning maximum proton energy for applications and identifying key areas for future in-depth research.

Our optimization method can be extended to other metrics. For example, optimizing proton flux (protons/sr) can be challenging due to high shot-to-shot fluctuations ($\sim$18%). This variability complicates the assessment of optimization strategies. A potential solution is to incorporate statistical analysis and robust experimental design to reduce fluctuations. As demonstrated, our approach is particularly valuable for applications where achieving high proton energy is the primary goal. MSBO also improved mean and total proton energy, beam charge, and hot electron temperature. This study focused on cutoff energy due to its highest dynamic range, with the optimized configuration showing stability within experimental noise.

Our method is particularly valuable for facilities with limited diagnostic capabilities, as it circumvents the need for complex diagnostics to be able to measure wavefront at nominal energy. By leveraging data-driven methods, it offers a cost-effective and scalable solution for optimizing laser-driven ion acceleration, making it accessible to a wider range of high-power laser facilities.

In this work, we optimized 20 of 48 DM actuators for computational efficiency. Expanding to more actuators poses challenges for standard BO, as surrogate models struggle in high-dimensional spaces[28]. However, advanced surrogate models, parallelized BO, or hybrid optimization could extend their capabilities, potentially unlocking higher proton energies. Adapting our method for lower repetition rate facilities or limited target availability (for example, with less than 100 laser shots) could further enhance its applicability.

This framework enables resource-efficient optimization in laser-plasma acceleration, paving the way for more systematic and robust strategies. Future extensions could apply this framework to other laser-plasma interactions, reinforcing data-driven methods as essential tools in the field.

ACKNOWLEDGMENTS

The authors would like to thank the staff of the ALLS laser facility for the technical assistance during the experiment, in particular, Mandy Doly, Marc-André Picard, Stéphane Payeur, William Lévesque. We also acknowledge fruitful discussions with Arthur Santos Pimentel and Tiago Falk. We would like also to thank Baptiste Laveix from *Phasics* for his help with the SID4 software. We thank Simon Blackburn, Bruno Rousseau, and Jeremy Pinto from the Mila – Québec AI Institute for their valuable discussions and insights, which contributed meaningfully to the development of this work. This research is supported by the Canada Foundation for Innovation: Major Science Initiatives, Ministère de l'Économie, de l'Innovation et de l'Énergie du Québec, by the National Sciences and Engineering Research Council of Canada (NSERC) (Grant — RGPIN-2023-05459, ALLRP 556340 – 20) and Compute Canada (Job: pve-323-ac).

DATA AVAILABILITY STATEMENT

The data that support the findings of this study are available from the corresponding author upon reasonable request.

REFERENCES

[1]M. Borghesi, A. Bigongiari, S. Kar, and et al., "Laser-driven proton acceleration: source optimization and radiographic applications," Plasma Physics and Controlled Fusion **50**, 124040 (2008).
[2]C.-M. Ma, I. Veltchev, E. Fourkal, and et al., "Development of a laser-driven proton accelerator for cancer therapy," Laser Physics **16**, 639–646 (2006).
[3]B. J. Galow, Z. Harman, and C. H. Keitel, "Intense high-quality medical proton beams via laser fields," Opt. Express **18**, 25950–25957 (2010).
[4]M. Passoni, F. M. Arioli, L. Cialfi, and et al., "Advanced laser-driven ion sources and their applications in materials and nuclear science," Plasma Physics and Controlled Fusion **62**, 014022 (2019).
[5]M. Barberio, M. Scisciò, S. Vallières, and et al., "Laser-accelerated particle beams for stress testing of materials," Nat. Commun. **9**, 372 (2018).
[6]M. Passoni, L. Fedeli, and F. Mirani, "Superintense laser-driven ion beam analysis," Scientific Reports **9**, 9202 (2019).
[7]P. Puyuelo-Valdes, S. Vallières, M. Salvadori, and et al., "Combined laser-based x-ray fluorescence and particle-induced x-ray emission for versatile multi-element analysis," Scientific Reports **11**, 9998 (2021).
[8]M. Barberio and P. Antici, "Laser-pixe using laser-accelerated proton beams," Sci. Rep. **9**, 1–9 (2019).
[9]M. Barberio, S. Veltri, M. Scisciò, and P. Antici, "Laser-accelerated proton beams as diagnostics for cultural heritage," Sci. Rep. **7**, 40415 (2017).
[10]M. Roth, T. Cowan, M. Key, and et al., "Fast ignition by intense laser-accelerated proton beams," Phys. Rev. Lett **86**, 436 (2001).
[11]P. Patel, A. Mackinnon, M. Key, and et al., "Isochoric heating of solid-density matter with an ultrafast proton beam," Phys. Rev. Lett **91**, 125004 (2003).
[12]P. Antici, J. Fuchs, S. Atzeni, and et al., "Isochoric heating of matter by laser-accelerated high-energy protons," in *Journal de Physique IV (Proceedings)*, Vol. 133 (EDP sciences, 2006) pp. 1077–1079.
[13]T. Ziegler, I. Göthel, S. Assenbaum, and et al., "Laser-driven high-energy proton beams from cascaded acceleration regimes," Nature Physics **20**, 1211–1216 (2024).
[14]H. Cheng, Y. Z. Li, Y. Yan, and et al., "Modulation of laser-driven proton beams in underdense plasma," Physics of Plasmas **31**, 123105 (2024), https://pubs.aip.org/aip/pop/article-pdf/doi/10.1063/5.0217978/20295945/123105_1_5.0217978.pdf.
[15]H. Y. Al-Omari, M. E. Yahia, and A. M. Almomani, "Laser-driven acceleration of a 94.8 mev uniform proton beam enhanced by a thin axial absorber rod," Phys. Rev. Accel. Beams **27**, 073501 (2024).
[16]P. Antici, M. Fazi, A. Lombardi, and et al., "Numerical study of a linear accelerator using laser-generated proton beams as a source," Journal of Applied Physics **104** (2008).
[17]P. Antici, M. Migliorati, A. Mostacci, and et al., "A compact post-acceleration scheme for laser-generated protons," Physics of Plasmas **18** (2011).
[18]S. Wilks, A. Langdon, T. Cowan, and et al., "Energetic proton generation in ultra-intense laser-solid interactions," Phys. Plasmas **8**, 542–549 (2001).
[19]R. Anirudh, R. Archibald, M. S. Asif, M. M. Becker, S. Benkadda, P.-T. Bremer, R. H. Budé, C.-S. Chang, L. Chen, R. Churchill, *et al.*, "2022 review of data-driven plasma science," IEEE Transactions on Plasma Science **51**, 1750–1838 (2023).
[20]A. Döpp, C. Eberle, S. Howard, and et al., "Data-driven science and machine learning methods in laser–plasma physics," High Power Laser Science and Engineering **11**, e55 (2023).
[21]R. Roussel, A. L. Edelen, T. Boltz, and et al., "Bayesian optimization algorithms for accelerator physics," Physical review accelerators and beams **27**, 084801 (2024).
[22]Y.-L. Liu, Y.-C. Chen, C.-S. Jao, and et al., "Deep learning approaches for modeling laser-driven proton beams via phase-stable acceleration," Physics of Plasmas **31** (2024), https://doi.org/10.1063/5.0178238.

[23]C. J. McQueen, R. Wilson, T. P. Frazer, and et al., "A neural network-based synthetic diagnostic of laser-accelerated proton energy spectra," Communications Physics **8**, 66 (2025).
[24]D. R. Jones, M. Schonlau, and W. J. Welch, "Efficient global optimization of expensive Black-Box functions," Journal of Global Optimization **13**, 455–492 (1998).
[25]B. Shahriari, K. Swersky, Z. Wang, and et al., "Taking the human out of the loop: A review of bayesian optimization," Proceedings of the IEEE **104**, 148–175 (2016).
[26]E. Brochu, V. M. Cora, and N. De Freitas, "A tutorial on bayesian optimization of expensive cost functions, with application to active user modeling and hierarchical reinforcement learning," arXiv preprint arXiv:1012.2599 (2010), https://doi.org/10.48550/arXiv.1012.2599.
[27]J. Mockus, "The bayesian approach to global optimization," in *System Modeling and Optimization: Proceedings of the 10th IFIP Conference New York City, USA, August 31–September 4, 1981* (Springer, 2005) pp. 473–481.
[28]P. I. Frazier, "A tutorial on bayesian optimization," arXiv preprint arXiv:1807.02811 (2018), https://doi.org/10.48550/arXiv.1807.02811.
[29]J. Duris, D. Kennedy, A. Hanuka, and et al., "Bayesian optimization of a free-electron laser," Phys. Rev. Lett. **124**, 124801 (2020).
[30]S. Jalas, M. Kirchen, P. Messner, and et al., "Bayesian optimization of a laser-plasma accelerator," Phys. Rev. Lett. **126**, 104801 (2021).
[31]R. J. Shalloo, S. J. D. Dann, J.-N. Gruse, C. I. D. Underwood, A. F. Antoine, C. Arran, M. Backhouse, C. D. Baird, M. D. Balcazar, N. Bourgeois, J. A. Cardarelli, P. Hatfield, J. Kang, K. Krushelnick, S. P. D. Mangles, C. D. Murphy, N. Lu, J. Osterhoff, K. Põder, P. P. Rajeev, C. P. Ridgers, S. Rozario, M. P. Selwood, A. J. Shahani, D. R. Symes, A. G. R. Thomas, C. Thornton, Z. Najmudin, and M. J. V. Streeter, "Automation and control of laser wakefield accelerators using bayesian optimization," Nature Communications **11**, 6355 (2020).
[32]F. Irshad, S. Karsch, and A. Döpp, "Multi-objective and multi-fidelity bayesian optimization of laser-plasma acceleration," Phys. Rev. Res. **5**, 013063 (2023).
[33]S. Jalas, M. Kirchen, C. Braun, and et al., "Tuning curves for a laser-plasma accelerator," Phys. Rev. Accel. Beams **26**, 071302 (2023).
[34]B. Loughran, M. J. Streeter, H. Ahmed, and et al., "Automated control and optimization of laser-driven ion acceleration," High Power Laser Science and Engineering **11**, e35 (2023).
[35]Y. Gao, J. Bin, D. Haffa, and et al., "An automated, 0.5 hz nano-foil target positioning system for intense laser plasma experiments," High Power Laser Science and Engineering **5**, e12 (2017).
[36]F. Treffert, C. B. Curry, H.-G. Chou, and et al., "High-repetition-rate, multi-mev deuteron acceleration from converging heavy water microjets at laser intensities of 1021 w/cm2," Applied Physics Letters **121** (2022), https://doi.org/10.1063/5.0098973.
[37]L. Giuffrida, F. Schillaci, F. Grepl, and et al., "Commissioning experiments at the elimaia user beamline (conference presentation)," in *Laser Acceleration of Electrons, Protons, and Ions VII* (SPIE, 2023) p. PC125790S.
[38]R. Nedbailo, J. Park, R. Hollinger, and et al., "Compact high repetition rate thomson parabola ion spectrometer," Review of Scientific Instruments **94** (2023), https://doi.org/10.1063/5.0101859.
[39]M. Nishiuchi, I. Daito, M. Ikegami, and et al., "Focusing and spectral enhancement of a repetition-rated, laser-driven, divergent multi-mev proton beam using permanent quadrupole magnets," Applied Physics Letters **94** (2009), https://doi.org/10.1063/1.3078291.
[40]E. Catrix, F. Boivin, K. Langlois, and et al., "Stable high repetition-rate laser-driven proton beam production for multidisciplinary applications on the advanced laser light source ion beamline," Review of Scientific Instruments **94** (2023), https://doi.org/10.1063/5.0160783.
[41]P. Sprangle, E. Esarey, and A. Ting, "Nonlinear theory of intense laser-plasma interactions," Physical review letters **64**, 2011 (1990).
[42]P. Kaw, "Nonlinear laser–plasma interactions," Reviews of Modern Plasma Physics **1**, 1–42 (2017).
[43]B. Beaurepaire, A. Vernier, M. Bocoum, and et al., "Effect of the laser wave front in a laser-plasma accelerator," Physical Review X **5**, 031012 (2015).
[44]T. Kurz, T. Heinemann, M. Gilljohann, and et al., "Demonstration of a compact plasma accelerator powered by laser-accelerated electron beams," Nature communications **12**, 2895 (2021).
[45]J. Lin, Y. Ma, R. Schwartz, and et al., "Adaptive control of laser-wakefield accelerators driven by mid-ir laser pulses," Optics Express **27**, 10912–10923 (2019).
[46]W. Wang, "Proton acceleration driven by relativistic femtosecond laguerre–gaussian lasers," Reviews of Modern Plasma Physics **8**, 1–29 (2024).
[47]C. Brabetz, S. Busold, T. Cowan, and et al., "Laser-driven ion acceleration with hollow laser beams," Physics of Plasmas **22** (2015), https://doi.org/10.1063/1.4905638.
[48]C. Willim, J. Vieira, V. Malka, and L. O. Silva, "Proton acceleration with intense twisted laser light," Physical Review Research **5**, 023083 (2023).
[49]S. Vallières, M. Salvadori, P. Puyuelo-Valdes, and et al., "Thomson parabola and time-of-flight detector cross-calibration methodology on the alls 100 tw laser-driven ion acceleration beamline," Review of Scientific Instruments **91** (2020), https://doi.org/10.1063/5.0020257.
[50]J. L. Speiser, M. E. Miller, J. Tooze, and et al., "A comparison of random forest variable selection methods for classification prediction modeling," Expert systems with applications **134**, 93–101 (2019).
[51]C. Rea, R. Granetz, K. Montes, and et al., "Disruption prediction investigations using machine learning tools on diii-d and alcator c-mod," Plasma Physics and Controlled Fusion **60**, 084004 (2018).
[52]A. Piccione, J. Berkery, S. Sabbagh, and et al., "Physics-guided machine learning approaches to predict the ideal stability properties of fusion plasmas," Nuclear Fusion **60**, 046033 (2020).
[53]M. D. Shields and J. Zhang, "The generalization of latin hypercube sampling," Reliability Engineering & System Safety **148**, 96–108 (2016).
[54]J. C. Helton and F. J. Davis, "Latin hypercube sampling and the propagation of uncertainty in analyses of complex systems," Reliability Engineering & System Safety **81**, 23–69 (2003).
[55]S.-O. Contributors, "skopt.gp_minimize — scikit-optimize documentation," (2025), accessed: 2025-01-17.
[56]F. Hutter, H. H. Hoos, and K. Leyton-Brown, "Sequential model-based optimization for general algorithm configuration," in *Learning and intelligent optimization: 5th international conference, LION 5, rome, Italy, January 17-21, 2011. selected papers 5* (Springer, 2011) pp. 507–523.
[57]J. Fuchs, P. Antici, E. d'Humières, and et al., "Laser-driven proton scaling laws and new paths towards energy increase," Nature physics **2**, 48–54 (2006).